JOURNAL OF COMPUTATIONAL PHYSICS 75, 86–102 (1988)

Interpolating and Integrating Three-Point Correlation Functions on a Lattice

JAMES G. BERRYMAN

Lawrence Livermore National Laboratory,
University of California,
P. O. Box 808 L-156 Livermore, California 94550

Received January 30, 1987; revised April 17, 1987

Various methods of estimating effective properties of composite materials require information about microgeometry contained in the statistical three-point correlation functions. If these three-point correlation functions are measured using digital image processing techniques, the values are computed for a discrete set of admissible triangular arguments corresponding to triangles whose vertices are commensurate with a square lattice. To extract the desired geometrical information from the correlation functions, methods of interpolating and integrating between these lattice-based correlation function values must be developed. In previous work, a minimal subset of the lattice-commensurate triangles was proposed as the primary data set. However, to obtain sufficient accuracy in the interpolations, it has been found necessary to expand the primary set of lattice-commensurate triangles to include other triangles. The size of the new set of triangles is less than a factor of two larger than that of the previous set; yet this set has the distinct advantage that a sorting and storing algorithm mapping the triangular arguments onto a compact one-dimensional array depends on formulas known in closed form. The spline interpolation algorithm maintains the shape of the argument triangle while (1) scaling its longest side to an integer number of pixel widths, (2) following with either bilinear or biquadratic interpolation through lattice points surrounding the third vertex, and finally (3) completing the estimate with a quadratic Newton forward-difference interpolation in the triangle scale size. Statistical comparison with exact values for the penetrable sphere model shows that this interpolation scheme provides accurate estimates of S_3 off the grid points; better than $\pm 0.02\%$ accuracy is typical for a quadratic interpolation scheme. These interpolated values are subsequently used in a Monte Carlo integration scheme developed previously for various 3D integrals of S_3 and the results are comparable to those obtained with the exact S_3 for penetrable spheres.

I. INTRODUCTION

It has recently been proposed that the statistical data required for various applications to composite materials [1] be obtained using digital image processing techniques [2]. This appoach allows quantitative determination of volume fraction data, of interface area per unit volume, and of more sophisticated measures of the topology of material mixtures including the n-point spatial correlation functions. It has been demonstrated that the two-point and three-point correlation functions can

0021-9991/88 $3.00

be measured quite accurately both for synthetic materials [2] and for real materials such as porous sandstones [3].

Since these correlation functions are determined from the digital images, the correlation data gathered necessarily form a discrete set. In particular, the digital images are normally composed of square arrays of picture elements (or pixels) and the natural basis for the correlation measurements is the distance separating the pixel centers. The correlation values obtained are those for lengths commensurate with the underlying square lattice, i.e., lattice points separated by exactly these distance can be found.

The correlation functions are themselves only an intermediate step in the process of determining the desired statistical properties of the composite. To obtain the final results, the correlation functions must be used as the integrand of some complex integrals. The purpose of this paper is therefore to develop methods for interpolating between the measured values of the correlation functions, and then to use these interpolated values in the integrals needed to find the desired measures of the composite's microgeometry. To obtain sufficient accuracy in the interpolations for the required (conditionally convergent) integrations, it has been found necessary to expand the set of lattice-commensurate traingles beyond the minimal subset originally proposed [2]. The size of the new set of argument triangles is less than a factor of two larger than that of the previous set; yet this set has the distinct advantage that the sorting and storing algorithm, which maps the triangles onto a compact one-dimensional array, depends on formulas which are obtained here in closed form.

Quadratic spline interpolation is used for all three arguments of the three-point correlation function. The microgeometry parameters computed using the interpolated functions then agree with the exact values within the statistical error of the Monte Carlo integration method.

II. Spatial Correlation Functions

A discussion of the significance of the spatial correlation functions has been presented recently, together with a detailed analysis of methods for obtaining these functions experimentally using image processing techniques [2]. We will not repeat the detailed discussion here, but it is still necessary to define the correlation functions and mention their relevant properties. The discussion is limited to two-phase composite media.

Let $p(\mathbf{x})$ be the value of some property of a random composite material (e.g., electrical or thermal conductivity, dielectric constant, bulk or shear modulus, etc.) which assumes one of two values p_0 or p_1 depending on whether $\mathbf{x}$ is located in a grain of material 0 or material 1. Define the indicator or characteristic function

$$f(\mathbf{x}) = \frac{p(\mathbf{x}) - p_0}{p_1 - p_0}. \tag{1}$$

Then $f(\mathbf{x})=0$ in material 0 and $f(\mathbf{x})=1$ in material 1. For example, in a porous medium we may arbitrarily label all solid regions as material 0 and all void regions as material 1. Since complete knowledge of the stochastic variable f is seldom available, our interest in the characteristic function is generally limited to a few of its statistical properties. If chosen properly, these quantities are often sufficient to provide the data needed for variational bounds on the macroscopic average of the property being studied [1].

The first three spatial correlation functions are defined by

$$\hat{S}_1 = \langle f(\mathbf{x}) \rangle = \phi_1, \tag{2}$$

$$\hat{S}_2(\mathbf{r}_1, \mathbf{r}_2) = \langle f(\mathbf{x}+\mathbf{r}_1) f(\mathbf{x}+\mathbf{r}_2) \rangle, \tag{3}$$

and

$$\hat{S}_3(\mathbf{r}_1, \mathbf{r}_2, \mathbf{r}_3) = \langle f(\mathbf{x}+\mathbf{r}_1) f(\mathbf{x}+\mathbf{r}_2) f(\mathbf{x}+\mathbf{r}_3) \rangle. \tag{4}$$

The brackets $\langle \cdot \rangle$ indicate a volume average over the spatial coordinate $\mathbf{x}$. The volume fraction of constituent 1 is given by ϕ_1. We will refer to the three correlation functions defined this way as the one-, two-, and three-point correlation functions, respectively. Since two points lie along a line and three points lie in a plane, the two-point and three-point correlations (as well as the one-point correlation) may be measured by processing digital images of material cross sections. In the present paper, we will stress the three-point correlation functions. In general, we assume that the composite medium of interest is statistically homogeneous so that on average only the differences in the coordinate values are significant (translational invariance). Furthermore, we often assume that the microstructure of the material being studied is statistically isotropic on a local scale so that appropriate local averges do not depend on the orientation of the arguments. (An example of local isotropy in conjunction with global anisotropy is a material with transversely isotropic microstructure composed of thin layers each having isotropic microstructure. Such a material can be treated if the correlation functions are determined by examining cross sections taken perpendicular to the axis of symmetry.) With these assumptions, we find that the two-point correlation function simplifies to

$$\hat{S}_2(\mathbf{r}_1, \mathbf{r}_2) = \tilde{S}_2(\mathbf{r}_{12}) = S_2(r_{12}), \tag{5}$$

while the three-point correlation function satisfies

$$\hat{S}_3(\mathbf{r}_1, \mathbf{r}_2, \mathbf{r}_3) = \tilde{S}_3(\mathbf{r}_{12}, \mathbf{r}_{13}) = S_3(r_{12}, r_{13}, \mu_{12,13}), \tag{6}$$

where

$$\mathbf{r}_{ij} = \mathbf{r}_j - \mathbf{r}_i, \; r_{ij} = |\mathbf{r}_{ij}|,$$

and

$$\mu_{ij,ik} = \cos\theta = \mathbf{r}_{ij} \cdot \mathbf{r}_{ik} / r_{ij} r_{ik}.$$

The two-point correlation $S_2(x)$ is the probability that two points a distance $x = r_{12}$ apart are both in material 1. The three-point correlation function $S_3(x, y, \mu)$ is the probability that all three vertices of the triangle determined by (x, y, μ) lie in material 1.

In a random material possessing no long range order, we have

$$\lim_{y \text{ fixed}, x \to \infty} S_3(x, y, \mu) = \phi S_2(y) \tag{7}$$

and

$$\lim_{x, y \to \infty} S_3(x, y, \mu) = \phi^3, \tag{8}$$

assuming that $\mu \neq 1$ or that the difference $x - y$ is not fixed if $\mu = 1$. A most important property of S_3 for statistically homogeneous and isotropic media is the fact that the value depends only on the size and shape of the triangle formed by its arguments, not on the orientation of that triangle. Thus,

$$S_3(r_{12}, r_{13}, \mu_{12,13}) = S_3(r_{21}, r_{23}, \mu_{21,23}) = S_3(r_{31}, r_{32}, \mu_{31,32}). \tag{9}$$

Furthermore, the order of the first two arguments may be freely interchanged. It is important to account for the symmetries (9) when designing a scheme to calculate, sort, and store the values of S_3, otherwise the stored values could be as much as sixfold degenerate.

In general, these spatial correlation functions must be determined empirically. These one-, two-, and three-point correlation functions may be found using digital image processing techniques described previously [2]. However, during code development, it is very helpful to have an analytical model of these correlation functions for some realizable two-phase composite. The penetrable sphere model provides such an example. This model is composed of points distributed randomly in three-dimensions; these points form the centers of spheres of arbitrary but uniform radius. The sphere interiors are considered regions of material 0, while regions exterior to all spheres are regions of material 1. Because the sphere centers are uncorrelated, all the correlation functions may be determined analytically [2]. This model will be used extensively in the following sections to check the accuracy of our interpolation and integration schemes.

III. Sorting and Storing

For digital image processing, it is clearly advantageous to compute S_3 only for those values whose triangular argument lies exactly on three lattice points. However, we need not blindly compute S_3 for every lattice-commensurate triangle. One scheme has already been proposed [2] for choosing a minimal subset of all lattice-commensurate triangles; this scheme was believed to be adequate for purposes of interpolation. The scheme is summarized in the following paragraphs.

Original Algorithm

A minimal set of lattice-commensurate triangles is uniquely determined by the following algorithm: Each triangle will be labelled by three integers (l, m, n). The first integer l is the length of the longest side of the triangle measured in units of pixel width. The vertex formed by the intersection of the longest side and the shortest side of this triangle is then treated as the origin $(0, 0)$ of an (m, n) coordinate system. The longest side of the triangle is placed along the m-axis so that the second vertex is located at $(l, 0)$. The third vertex of the triangle is then located in the first quadrant at (m, n).

All triangles whose longest side is an integer number of pixel widths may be sorted in this manner. The third vertex specified by (m, n) will always lie in a sector of a circle of radius l centered at $(l, 0)$, bounded below by the m-axis, and on the right by the line $m = l/2$. The arc occurs because the side of intermediate length can be equal to but never longer than l. The line at $m = l/2$ occurs because the smallest side can be equal to but never longer than the intermediate side; furthermore, since the triangle with vertex $(l-m, n)$ has the same shape as the one at (m, n), we have reflection symmetry across the line $m = l/2$. Note that, although all right triangles with integer length sides adjacent to the right angle are lattice-commensurate triangles, these right triangles have *not* been included in this "minimal subset" because the corresponding value of S_3 lies within a pixel width of those values contained in the minimal subset.

Modified Algorithm

It has been found that, when interpolation is attempted between general triangles using the set of lattice-based triangles provided by this original algorithm, the accuracy is not adequate for the complex integrals to be evaluated. The main problem is illustrated in Fig. 1. The minimal subset of triangles included in the original algorithm corresponds to those lattice points lying in the cross-hatched region of the diagram. If we need to evaluate S_3 for triangles whose side of intermediate length is comparable to that the longest side, then the third vertex will fall in a region of (m, n) where it cannot easily be surrounded by four points with known correlation function values (such poorly determined points lie in the regions of double cross-hatching in Fig. 1). We can resolve this difficulty by expanding the original data set to guarantee that any such point is surrounded by points with known values; such an expansion forces us to compute and store more than the minimal subset of S_3 values, i.e., all the triangles determined by the vertices lying in the rectangles of Fig. 1. Nevertheless, the new set is significantly simpler to use in computations because the algorithm for sorting and storing can be determined in closed form. In general, we choose triangles labelled (l, m, n) for those values which satisfy

$$0 \leqslant m \leqslant \lceil l/2 \rceil \tag{10}$$

and

$$0 \leqslant n \leqslant l, \tag{11}$$

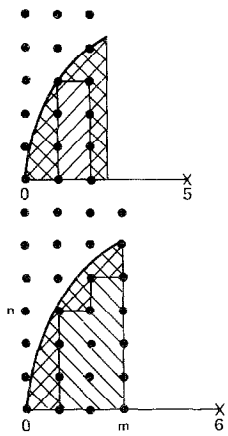

FIG. 1. Illustrating the problem of accurate interpolation based on the minimal set of lattice-commensurate triangles (with vertices at lattice points lying in the cross-hatched region). Although points close to the boundaries (in the doubly cross-hatched region) lie within one pixel of an included lattice point, they are not surrounded by such points. There are also not enough known points available for accurate extrapolation. The modified algorithm solves this problem by including triangles with vertices at all lattice points in the rectangle as shown.

where the operator $[\cdot]$ truncates the argument to the largest integer value. The new set is illustrated for $l \leqslant 8$ in Fig. 2.

Next we need to find an efficient method of addressing the triangles labelled by the triple (l, m, n). We choose to assign the addresses $I_{l,m,n}$ so that (i) all addresses with fixed l are contiguous, (ii) for given l all addresses with fixed m are contiguous, and (iii) $I_{l,m,n}$ increases whenever l, m, or n increase. If the total storage requirement T_l for all triangles with largest side less than or equal to l is determined by the recursion

$$T_l = T_{l-1} + ([l/2] + 1)(l + 1) \tag{12}$$

with $T_{-1} = 0$, then clearly we have $I_{l+1,0,0} = T_l + 1$. It follows that

$$I_{l+1,0,0} = I_{l,0,0} + ([l/2] + 1)(l + 1). \tag{13}$$

Using these facts, we can easily generate Table I. Now it is possible to solve these recursion relations for the general expressions satisfied by the addresses $I_{l,0,0}$ or for the storage requirement I_l. In the process of doing so, certain identities appear which are useful for checking the results. For example, we can easily show for even $l \geqslant 2$ that

$$I_{l,0,0} = I_{l-2,0,0} + l^2 - l/2 \tag{14}$$

and

$$I_{l+1,0,0} = I_{l-1,0,0} + l^2 + 3l/2 + 1, \tag{15}$$

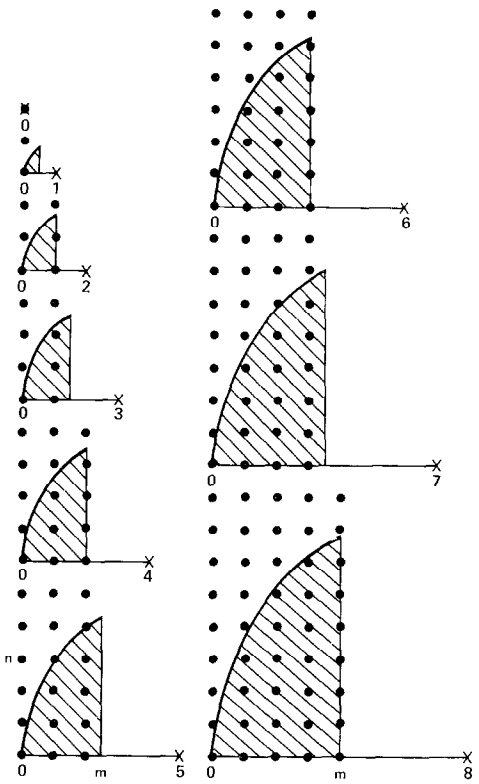

FIG. 2. Illustrating the expanded set of lattice-commensurate triangles used by the modified algorithm for $l \leqslant 8$. The Monte Carlo integration scheme chooses triangles whose third vertex lies somewhere in one of the cross-hatched regions. These vertices are now surrounded by lattice points with known values, directly for l even and/or by symmetry around $m = [l/2]$ for l odd.

where $I_{0,0,0} = 1$ and $I_{1,0,0} = 2$. The general expressions for the addresses are then given by

$$I_{l,0,0} = l^3/6 + 3l^2/8 + l/12 + 1 \tag{16}$$

and

$$I_{l+1,0,0} = l^3/6 + 7l^2/8 + 19l/12 + 2 \tag{17}$$

for even $l \geqslant 0$. It is straightforward to check that these expressions (16) and (17) satisfy the constraints (13)–(15) listed above. Finally, the general expression for an arbitrary address is given by

$$I_{l,m,n} = I_{l,0,0} + m(l+1) + n. \tag{18}$$

Thus, (16)–(18) provide a convenient algorithm for mapping the expanded subset of lattice-commensurate triangles onto a one-dimensional array.

TABLE I

Number of Triangles in a Convenient Set of Lattice-Commensurate Triangles with Longest Side Equal to l Units

l	No. of triangles	Storage requirement (T_l)	l	No. of triangles	Storage requirement (T_l)
0	1	1	19	200	1485
1	2	3	20	231	1716
2	6	9	21	242	1958
3	8	17	22	276	2234
4	15	32	23	288	2522
5	18	50	24	325	2847
6	28	78	25	338	3185
7	32	110	26	378	3563
8	45	155	27	392	3955
9	50	205	28	435	4390
10	66	271	29	450	4840
11	72	343	30	496	5336
12	91	434	31	512	5848
13	98	532	32	561	6409
14	120	652	48	1225	20525
15	128	780	64	2145	47377
16	153	933	96	4753	155673
17	162	1095	128	8385	364065
18	190	1285			

Note. The cumulative total for all cases with longest side less than or equal to l determines the required storage capacity T_l. Note that, for a single image with 512×512 pixels, triangle size has been restricted in the text to $l \leqslant 64$ to avoid storing more values of S_3 than the total number of pixels in the original image.

IV. Interpolation Schemes

In this section, we will follow the convention that lower case roman symbols in the range $i, \ldots, n$ refer to dimensionless integers and lower case greek symbols refer to dimensionless real numbers, while capital roman symbols $H, \ldots, T$ are real numbers with dimensions of length. Now for a triangle with sides $R \leqslant S \leqslant T$, we define the triple (L, M, N) by

$$L = T, \tag{19}$$

$$M = (R^2 + T^2 - S^2)/2T = R \cos \theta, \tag{20}$$

and

$$N = (R^2 - M^2)^{1/2} = R \sin \theta. \tag{21}$$

The angle θ is the angle between the sides of length R and T.

For interpolation and integration, we will measure all triangle lengths in units of pixel size H. Then, the normalized triple $(L/H, M/H, N/H)$ will not generally fall on any of the lattice-commensurate triangles defined in Section III. When the triangle is commensurate with the lattice (i.e., $(l, m, n) = (L/H, M/H, N/H)$, where l, m, n are all integers), the lattice-commensurate values V are stored in a linear array following the rule

$$V(I_{l,m,n}) = S_3(R, T, \cos\theta). \tag{22}$$

If the triangle is not commensurate with the lattice, then interpolation is required. We will interpolate between the known values of the three-point correlation function in two stages. In doing so, we maintain the shape of the triangle, but scale its size so that the longest side of the scaled triangles is an integer in pixel-width units. (1) First, we obtain an interpolated value for the correlation function of the scaled triangles by interpolation in (m, n) for fixed l. (2) Then, we interpolate between the reference values of l to obtain our estimate of the correlation function for the triangle of the correct size and shape. This procedure amounts to interpolating along a one-dimensional slice through the three-dimensional function using triangle shape to fix the ratio of the lengths of two sides and the angle between them, while a size multiplier serves as the remaining free variable.

The reference values for l are obtained from the largest integer in L/H,

$$l = [L/H]. \tag{23}$$

In scaling the triangle, we shrink it by a factor of lH/L and expand it by factors of $(l+1)\,H/L$ and $(l+2)\,H/L$. For example, if

$$\mu_k = kM/L \qquad \text{and} \qquad \nu_k = kN/L, \tag{24}$$

where $k = l$, $l+1$, or $l+2$, then the interpolation points closest to the origin in each of the three scaled triangles are located by

$$m_k = [\mu_k], \qquad n_k = [\nu_k]. \tag{25}$$

Since each pixel in the digitized image corresponds to a unit square of constant value, several methods of interpolation suggest themselves: (1) nearest neighbor interpolation, (2) bilinear interpolation, and (3) biquadratic interpolation. For real digital images, nearest neighbor interpolation is consistent with the discrete nature of the measured correlation function, but the algorithm for such an interpolation scheme for lattice-commensurate triangles is not very accurate. We prefer either bilinear or biquadratic interpolation because, for the examples of correlation functions that we can compute exactly (i.e., the penetrable sphere models [2]), these interpolants can be compared directly to the exact values at the intermediate points. Quadratic interpolation in triangle size is easily implemented for both methods. Thus, we have an ideal method of checking the accuracy of our interpolation and integration schemes if we use either bilinear or biquadratic inter-

polation. For bilinear interpolation, the four interpolation points typically used for a triangle with longest side k are (m_k, n_k), (m_k, n_k+1), (m_k+1, n_k), and (m_k+1, n_k+1). For biquadratic interpolation, the nine interpolation points normally used fall in the square with corners given by (m_k, n_k), (m_k, n_k+2), (m_k+2, n_k), and (m_k+2, n_k+2). We have tested both the bilinear and the biquadratic interpolation schemes in our integration routines (see Section V). We found that the accuracy of the bilinear interpolation was sufficient to calculate the ζ Milton number, but not so for the η Milton number. We will therefore present only the biquadratic interpolation scheme since it is the more general.

For fixed k and m, the quadratic interpolation for $n_k \leqslant \nu_k \leqslant n_k+1$ is given in terms of the stored values V by the Newton forward-difference [4, 5]

$$\Phi^{(f)}_{k,m} = V(I_{k,m,n_k+1}) + \tfrac{1}{2}[V(I_{k,m,n_k+2}) - V(I_{k,m,n_k})](\nu_k - 1 - n_k) + \tfrac{1}{2}[V(I_{k,m,n_k+2}) + V(I_{l,m,n_k}) - 2V(I_{k,m,n_k+1})](\nu_k - 1 - n_k)^2 \quad (26)$$

as long as the restriction $n_k+2 \leqslant k$ is satisfied. If instead we have $k < n_k+2$, then we must use the Newton-backward difference

$$\Phi^{(b)}_{k,m} = V(I_{k,m,n_k}) + \tfrac{1}{2}[V(I_{k,m,n_k+1}) - V(I_{k,m,n_k-1})](\nu_k - n_k) + \tfrac{1}{2}[V(I_{k,m,n_k+1}) + V(I_{k,m,n_k-1}) - 2V(I_{k,m,n_k})](\nu_k - n_k)^2. \quad (27)$$

Then, the biquadratic estimate E_k of S_3 for fixed k is given generally by

$$E_k = \Phi_{k,m_k+1} + \tfrac{1}{2}(\Phi_{k,m_k+2} - \Phi_{k,m_k})(\mu_k - 1 - m_k) + \tfrac{1}{2}(\Phi_{k,m_k+2} + \Phi_{k,m_k} - 2\Phi_{k,m_k+1})(\mu_k - 1 - m_k)^2. \quad (28)$$

Equation (28) is appropriate as long as $m_k+2 \leqslant [l/2]$. Two special cases arise if $m_k+1 \leqslant [l/2] < m_k+2$, for then

$$\Phi_{k,m_k+2} = \Phi_{k,m_k+1} \quad (29)$$

for $m_k+1 < [l/2]$ while

$$\Phi_{k,m_k+2} = \Phi_{k,m_k} \quad (30)$$

for $m_k+1 = [l/2]$. Both (29) and (30) follow easily from the reflection symmetry as seen in Fig. 2.

If $m_k+1 > [l/2]$, we then recall that the symmetry is such that the values of S_3 are equal for the triangles corresponding to the triples (k, m_k, n_k) and (k, m_k+1, n_k). If we were to use only these two triangles in the bilinear interpolation, then the interpolant would be constant in the whole region $m_k \leqslant \mu_k \leqslant [l/2]$. To correct this deficiency, we also include information from the values for the triangles (k, m_k-1, n_k) and (k, m_k-1, n_k+1). Thus, the estimate of E_k is given for $m_k \leqslant \mu_k \leqslant [l/2] < m_k+1$ by

$$E_k = \Phi_{k,m_k} + \tfrac{1}{2}(\mu_k - m_k)(1 + m_k - \mu_k)(\Phi_{k,m_k} - \Phi_{k,m_k-1}), \quad (31)$$

for both the bilinear and the biquadratic interpolation schemes. If $m_k = 0$ and $m_k + 1 > [l/2]$, then we cannot use (28) or (31) but an adequate approximation is produced by taking $E_k = \Phi_{k, m_k}$.

When each of the three values E_k for $k = l$, $l+1$, and $l+2$ have been found, the first stage of our interpolation process is complete. Then, we interpolate in triangle size to the point $\lambda = L/H$ using a Newton forward-difference formula of the form

$$E_\lambda = E_{l+1} + \tfrac{1}{2}(E_{l+2} - E_l)(\lambda - l - 1) + \tfrac{1}{2}(E_{l+2} + E_l - 2E_{l+1})(\lambda - l - 1)^2. \quad (32)$$

Equation (32) completes the second and final stage of the interpolation scheme.

The interpolation scheme presented here works very well everywhere except near the origin, i.e., for triangles of small size (on the order of a single pixel). Then, an altogether different approach is required. Our solution to this problem is described in Appendix A.

To check the accuracy of our interpolation scheme, we have run some statistical tests during the execution of the integration routine using the three-point correlation functions for the penetrable sphere model. For the bilinear interpolation scheme with a volume fraction $\phi = 0.5$, $l \leqslant 32$, and the sphere radius chosen to correspond to about 14 pixels, we find that the absolute error for 16×10^4 interpolants of S_3 tends to be negative (i.e., the estimate is systematically low) with a magnitude (on average) less than 2×10^{-4} while the average of the absolute value for the relative error was about 6×10^{-4}. No relative errors were found to be larger than 1%, and only about one in one thousand were found to be larger than 0.5%. When $\phi < 0.5$, we found significantly more of the interpolants (up to 20%) had relative errors as high as 0.5%; we attribute this increase to the decrease in magnitude of S_3 itself. When $\phi > 0.5$, we found significantly less of the interpolants (typically none) had relative errors as high as 0.5%; again we attribute this decrease to the increase in magnitude of S_3. For the biquadratic interpolation scheme with volume fraction $\phi = 0.5$, $l \leqslant 64$, and the sphere radius chosen to correspond to about 11 pixels, we find that the absolute error on average had magnitude 2×10^{-5} and none of the interpolants had relative errors as high as 0.5%. We also compared our interpolants with results of approximate formulas [6] relating S_3 to products of values of S_2 such as $\hat{S}_3(r, s, t) \simeq S_2(r)\ S_2(s)/\phi$ and $\hat{S}_3(r, s, t) \simeq S_2(r)\ [S_2(s) + S_2(t)/2\phi]$, where $t = (r^2 + s^2 - 2rs\mu)^{1/2}$. Even the bilinear interpolants were uniformly better than these estimates.

V. Integrating S_3

Milton [7, 8] has introduced two parameters depending on the microgeometry of a composite through the three-point correlation function S_3. These two geometric parameters of interest for studies of electrical or thermal conductivities and elastic constants are

$$\zeta_1 = \lim_{\Delta \to 0} \lim_{\Delta' \to \infty} \frac{9}{2\phi_0 \phi_1} \int_\Delta^{\Delta'} dr \int_\Delta^{\Delta'} ds \int_{-1}^{+1} d\mu \frac{S_3(r, s, \mu)}{rs} P_2(\mu) \quad (33)$$

and

$$\eta_1 = \frac{5\zeta_1}{21} + \lim_{\Delta \to 0} \lim_{\Delta' \to \infty} \frac{150}{7\phi_0\phi_1} \int_{\Delta}^{\Delta'} dr \int_{\Delta}^{\Delta'} ds \int_{-1}^{+1} d\mu \frac{S_3(r, s, \mu)}{rs} P_4(\mu), \tag{34}$$

where $\phi_1 = \phi$, $\phi_0 = 1 - \phi_1$, and $P_2(\mu)$ and $P_4(\mu)$ are the Legendre polynomials of order 2 and 4 given, respectively, by

$$P_2(\mu) = \tfrac{1}{2}(3\mu^2 - 1)$$

and

$$P_4(\mu) = \tfrac{1}{8}(35\mu^4 - 30\mu^2 + 3).$$

The integrands of both integrals (33) and (34) are singular for small values of r, s and poorly behaved for large values of r, s. The conditional convergence of the integrals requires that the integration over μ be performed before allowing the limits of integration over τ and s to reach their ultimate values. The singularity at the origin may be handled easily by standard methods. To improve the rate of convergence at large values of the independent variables r and s, we add and subtract a term that can be integrated analytically giving

$$\zeta_1 = \phi_1 + \lim_{\Delta \to 0} \lim_{\Delta' \to \infty} \frac{9}{2\phi_0\phi_1} \int_{\Delta}^{\Delta'} dr \int_{\Delta}^{\Delta'} ds \int_{-1}^{+1} d\mu \frac{S_3(r, s, \mu) - \phi_1 S_2(t)}{rs} P_2(\mu) \tag{35}$$

and

$$\eta_1 = (5\zeta_1 + 16\phi_1)/21 + \lim_{\Delta \to 0} \lim_{\Delta' \to \infty} \frac{150}{7\phi_0\phi_1} \times \int_{\Delta}^{\Delta'} dr \int_{\Delta}^{\Delta'} ds \int_{-1}^{+1} d\mu \frac{S_3(r, s, \mu) - \phi_1 S_2(t)}{rs} P_4(\mu), \tag{36}$$

where $t = (r^2 + s^2 - 2rs\mu)^{1/2}$. The integrals of S_3 are then evaluated using the adaptive Monte Carlo integration procedure VEGAS [9] used previously for computing variational bounds on permeability for aggregates of hard spheres [10] and on elastic constants for penetrable spheres [11]. The details of the numerical method for applications to (35) and (36) have been discussed in Ref. [11]. The only added complication is that, when a value of S_3 is called by the integration routine, it is generated using (26)–(32) or the formulas in Appendix A. The results are summarized in Tables II and III.

For the penetrable sphere model, we have found that the Monte Carlo integration scheme works best for low values of ϕ_1, and worst for high values ϕ_1. The method is known to perform poorly when the absolute value of the integral is small and fails to converge at all if the integral actually vanishes. The values quoted in Table II are sums of an analytical part (known exactly) and the integral involving S_3 (see Eqs. (35) and (36)). Thus, for high values of ϕ_1, the relative

TABLE II

Comparison of the Computed ζ_1 Milton Numbers [7, 8] for the Penetrable Sphere Model

ϕ_1	ζ_1 (Linear)	ζ_1 (Quadratic)	ζ_1 (Berryman [11])	ζ_1 (Torquato *et al.* [12])
0.10	0.48	0.46	0.46	0.442
0.20	0.54	0.52	0.52	0.518
0.35	0.61	0.61	0.61	
0.50	0.70	0.70	0.71	0.711
0.65	0.75	0.78	0.80	
0.80	0.91	0.87	0.88	0.886
0.90	0.95	0.92	0.94	0.945

Note. The first and second ζ_1 columns show the values obtained using the lattice-based linear and quadratic algorithms described in Section IV. Triangles with longest side $l \leqslant 32$ were used for the linear interpolation scheme, while those for $l \leqslant 64$ were used for the quadratic scheme. The third column shows the values obtained using the same integration routine (VEGAS [9]), but the exact values of S_3 in the integrand [11]. The fourth column shows the corresponding values obtained by Torquato *et al.* [12] using a Gaussian quadrature routine together with the exact S_3 in the integrand.

contribution of the integral to the total can be quite small; whereas, for small values of ϕ_1, the relative contribution of the integral is significant. We find that the error in the integral itself may vary from 1–2% for $\phi_1 = 0.1$ up to as much as 10% for $\phi_1 = 0.9$. However, because the contribution of the integral to the total is decreasing in virtually the same proportion as the error is increasing, we find that the error in the final result remains essentially constant at ± 0.02 for ζ, and a little more for η over the range of volume fractions considered. We do not recommend Monte Carlo

TABLE III

Comparison of the Computed η_1 Milton Numbers [7, 8] for the Penetrable Sphere Model

ϕ_1	η_1 (Quadratic)	η_1 (Berryman [11])	η_1 (Torquato *et al.* [12])
0.10	0.38	0.35	0.342
0.20	0.47	0.43	0.416
0.35	0.54	0.54	
0.50	0.66	0.64	0.633
0.65	0.75	0.75	
0.80	0.88	0.85	0.851
0.90	0.94	0.92	0.925

routine (VEGAS [9]), but the exact values of S_3 in the integrand [11]. Triangles with longest side $l \leqslant 64$ were used in the interpolation scheme. The third column shows the corresponding values obtained by Torquato *et al.* [12] using a Gaussian quadrature routine together with the exact S_3 in the integrand.

integration when highly accurate calculations of these integrals are desired; however, this method is as accurate as we can ever expect our S_3 data to be on real materials. Furthermore, this method is most accurate in the region with $\phi_1 < 0.5$. where most data will be gathered for porous composites such as rocks. To improve the accuracy of the η integration, either the total number of data points needs to be increased substantially so that the largest triangles have side $l \simeq 128$ or a higher order spline interpolation may be required.

One very interesting observation about the results for ζ and η concerns the choice of image magnification. The digital image used to produce the empirical values of S_3 may or may not contain the level of detail required for accurate computation of these integrals. Using triangles with longest side $l \leqslant 64$, we have found that our integration scheme produces good results for ζ when the effective radius R of the penetrable spheres satisfies $R/H \simeq 12$, where H is the pixel width. For η the best results were obtained when the effective radius of the penetrable spheres satisfied $R/H \simeq 25$. Thus, the image magnification required for the two integrals differs by about a factor of 2. This result is very reasonable when we compare the Legendre polynomials P_2 and P_4 appearing in the integrands. Since P_4 has twice as many zeroes as P_2, it is clear that, whatever image magnification is required to obtain accurate values of ζ, an image magnification about twice as large will be needed to obtain comparable accuracy for η. The observed behavior conforms to this expectation.

Although we might expect this factor of 2 difference in optimum image magnification to be maintained for real materials, we do not expect that these particular values of R/H (particle radius/pixel size) will be appropriate for all materials. The spherical particle shape and the lack of both cracks and surface roughness make the penetrable sphere model somewhat unrealistic. If the magnification of an image must be increased substantially beyond the values quoted in the preceding paragraph, then it is likely that the number of pixels in the image will also have to increase beyond the value of 512×512 assumed here. With the largest triangles having side $l \leqslant 64$, the total number of S_3 values computed from an image is 47,377. Increasing the largest triangle size by a factor of 2 means increasing the total number of S_3 values to 364,065 (see Table I); such an increase entails storing more computed values of S_3 than the total number of pixels in the original image. If such an increase in the data base is really needed for accurate determination of the integrals of interest, it might be preferable to use the digitized image itself as the data base for the larger triangles and compute the values of S_3 for these triangles as needed during execution of the integration routine. Another approach would be to increase the number of pixels per image to 1024×1024 or 2048×2048 directly or by constructing a mosaic. The method of spline interpolation presented here could be used with any of these approaches to the integration problem.

VI. Conclusions

We conclude that it is possible to produce interpolated values of the three-point correlation function from lattice-based measurements using the schemes presented in Section IV and Appendix A; these interpolants are sufficiently accurate to allow the conditionally convergent integrals of interest to converge. These interpolants may also be used in any integration scheme for the various integrals defining the geometric parameters of composite materials. For empirical values of the three-point correlation functions, we expect that the measurement error will generally far exceed the errors introduced by the interpolation scheme.

Appendix A

The interpolation schemes described in Section IV work well for the vast majority of triangular arguments. However, when the size of the triangles is so small that the longest side is comparable to the size of a pixel, a different approach is needed. In this region, we need to use all the information we have as efficiently as possible for two reasons: (1) The correlation function is changing rapidly and (2) there are very few data points for such small triangles. For the interpolation with $l \geqslant 2$, we can use nine data points (including symmetries) for each of the three l-values in our Newton forward-difference interpolation—for a total of 27 data points. However, from Table I, we see that the *total* number of data points gathered in this algorithm for $l \leqslant 2$ is only $T_2 = 9$; thus, this region requires special treatment.

For a triangle with sides $R \leqslant S \leqslant T$, we use the conventions of Section IV to define the triple (L, M, N) with values given by (19)–(21) and the normalized triple $(\lambda, \mu, \nu) = (L/H, M/H, N/H)$, where H is the pixel width. Then, the three-point correlation function is defined in terms of these arguments to be

$$\bar{S}_3(\lambda, \mu, \nu) = S_3(R, T, \cos\theta). \tag{A1}$$

Using this method of describing the triangular arguments, the three-point correlation function is known to possess the following symmetry properties:

$$\bar{S}_3(\lambda, 0, \nu) = \bar{S}_3(\nu, 0, \lambda) \tag{A2}$$

and

$$\bar{S}_3(\lambda, \mu, \nu) = F[\lambda, \nu, (\mu - \lambda/2)^2], \tag{A3}$$

where F is some function with three arguments. Equation (A2) is a statement of the fact that, if $\mu = 0$, the shape and size of the right-triangle argument are both preserved when λ and ν are interchanged. Equation (A3) states that, for fixed λ and ν, $\bar{S}_3(\lambda, \mu, \nu)$ is an even function of μ around the midpoint $\mu = \lambda/2$.

Using (A2) and (A3), we can construct a polynomial approximation for $\bar{S}_3(\lambda, \mu, \nu)$ possessing the appropriate symmetry properties. This approximation is

$$\begin{aligned}\bar{S}_3(\lambda, \mu, \nu) = a(1) + a(2)(\lambda + \nu) + a(3)\,\lambda^2 + a(4)\,\nu^2 \\ + a(5)\,\lambda\nu + a(6)\,\lambda\nu(\lambda + \nu) + a(7)\,\lambda^2\nu^2 \\ + (2\mu - \lambda)^2\,(a(8) + a(9)\,\nu^2).\end{aligned} \tag{A4}$$

Coefficients of λ and ν that have been combined directly to guarantee satisfaction of (A2) for arbitrary values. In addition, we also have the condition that

$$a(4) = a(3) + a(8). \tag{A5}$$

Thus, we have eight independent coefficients to be determined. These values can be found easily by excluding one of the available data points for $l \leqslant 2$, equating the polynomial to the remaining correlation function values at the grid points, and then solving recursively for the coefficients. We choose to exclude the data point for (2, 0, 2), since it is the one farthest from the region occupied by the minimal subset of lattice-commensurate triangles. The results for the coefficients are

$$\begin{aligned}a(1) &= \bar{S}_3(0, 0, 0), \\ a(4) &= \tfrac{1}{2}[\bar{S}_3(2, 0, 0) + a(1) - 2\bar{S}_3(1, 0, 0)], \\ a(2) &= \bar{S}_3(1, 0, 0) - a(1) - a(4), \\ a(3) &= \tfrac{1}{4}[\bar{S}_3(2, 1, 0) - a(1) - 2a(2)], \\ a(8) &= a(4) - a(3), \\ a(9) &= \tfrac{1}{4}[\bar{S}_3(2, 0, 1) - \bar{S}_3(2, 1, 1)] - a(8),\end{aligned}$$

and

$$\begin{aligned}a(5) &= 4x - 2y + z/4, \\ a(6) &= -2x + 3y/2 - z/4, \\ a(7) &= x - y + z/4,\end{aligned}$$

where

$$\begin{aligned}x &= \bar{S}_3(1, 0, 1) - a(1) - 2a(2) - 2a(4) - a(9), \\ y &= \bar{S}_3(2, 1, 1) - a(1) - 3a(2) - 4a(3) - a(4), \\ z &= \bar{S}_3(2, 1, 2) - a(1) - 4[a(2) + a(3) + a(4)].\end{aligned}$$

ACKNOWLEDGMENTS

I thank R. C. Y. Chin and G. W. Hedstrom for helpful comments on interpolation schemes and for suggesting the method of Monte Carlo integration. Work performed under the auspices of the U.S. Department of Energy by the Lawrence Livermore National Laboratory under Contract W-7405-ENG-48 and supported specifically by the Earth Sciences Department through the Institutional Research and Development Program and by the Electronics Engineering Department Thrust Area in Remote Sensing, Image, and Signal Engineering.

REFERENCES

1. M. J. BERAN, *Statistical Continuum Theories* (Interscience, New York, 1968), Chap. 6.
2. J. G. BERRYMAN, *J. Appl. Phys.* **57**, 2374 (1985).
3. J. G. BERRYMAN AND S. C. BLAIR, *J. Appl. Phys.* **60**, 1930 (1986).
4. F.B. HILDEBRAND, *Introduction to Numerical Analysis* (McGraw-Hill, New York, 1956), Chap. 4.
5. G. DAHLQUIST AND Å. Björck, *Numerical Methods* (Prentice-Hall, Englewood Cliffs, NJ. 1974), Sect. 7.3.
6. S. TORQUATO AND G. STELL, *Lett. Appl. Eng. Sci.* **23**, 375 (1985).
7. G. W. MILTON, *Phys. Rev. Lett.* **46**, 542 (1981).
8. G. W. MILTON, *J. Mech. Phys. Solids* **30**, 177 (1982).
9. G.P. LEPAGE, *J. Comput. Phys.* **27**, 192 (1978).
10. J. G. BERRYMAN, *J. Comput. Phys.* **52**, 142 (1983).
11. J. G. BERRYMAN, *J. Phys. D: Appl. Phys.* **18**, 585 (1985).
12. S. TORQUATO, G. STELL, AND J. BEASLEY, *Lett. Appl. Eng. Sci.* **23**, 385 (1985).